

POD-mode-augmented wall model and its applications to flows at non-equilibrium conditions

By C. Hansen[†], M. P. Whitmore, M. Abkar[†] AND X. I. A. Yang[‡]

Insights gained from the modal analysis are invoked for predictive large-eddy simulation (LES) wall modeling. Specifically, we augment the law of the wall (LoW) by an additional mode based on a one-dimensional scalar variant of the proper orthogonal decomposition (POD) applied to a 2D turbulent channel. As the constructed wall model contains two modes, i.e., the LoW mode and the POD-based mode, it requires LES information at two matching locations to solve the wall-shear stress. The model protects the LoW like the equilibrium wall model. *A-priori* tests show that the two modes, i.e., the LoW mode and the POD mode, yield a close approximation of the mean flow in flows with adverse and transverse pressure gradients. *A-posteriori* tests show that the POD-augmented wall model captures the initial decrease and the rapid decrease of the streamwise wall-shear stress in channels subjected to suddenly imposed adverse and transverse pressure gradients.

1. Introduction

The strict near-wall grid resolution requirement for large-eddy simulations (LESs) makes wall modeling a necessity at high Reynolds numbers (Yang & Griffin 2021). Figure 1 is a schematic of a wall-modeled LES (WMLES). The LES grid is coarse and scales with the boundary-layer thickness. The wall-shear stress is not computed per the discretization scheme. Rather, a wall model is employed. A wall model takes the LES information in the wall-adjacent cells and computes the wall-shear stress and wall heat flux. The most extensively used type of wall models are equilibrium-type models (Kawai & Larsson 2012; De Vanna *et al.* 2021). The models compute the wall fluxes according to some mean flow scaling, usually the law of the wall (LoW) in the wall-adjacent computational cell(s).

The LoW and equilibrium-type WMs fail when there are adverse pressure gradients (APGs) and transverse pressure gradient (TPGs). Both are common in real-world settings (Goc *et al.* 2021). Considerable work has been done to study the effects of APGs and TPGs (Monty *et al.* 2011; Volino 2020). Figure 2(a,b) is a schematic of two model problems (Na & Moin 1998; He & Seddighi 2015; Lozano-Durán *et al.* 2020), in which a 2D channel is subjected to a suddenly imposed APG or TPG. The flow decelerates in Figure 2(a) and turns in Figure 2(b). Relevant to near-wall turbulence modeling is the behavior of the mean flow (input to the wall model) and the wall-shear stress (output of the wall model). Figure 2(c) shows the evolution of the mean flow in Figure 2(a) after an APG, $f_x = 100f_{x,0}$, is suddenly imposed to a $Re_\tau = 1000$ channel. The mean velocity profile is above the LoW, and if one were to apply the LoW to predict the wall-shear stress, the wall-shear stress would be grossly overpredicted. Figure 2(d) shows the evolution of the x -direction wall-shear stress, τ_x , after a TPG, $f_z = 10f_{x,0}$, is applied to a

[†] Department of Mechanical and Production Engineering, Aarhus University, Denmark

[‡] Department of Mechanical Engineering, Pennsylvania State University

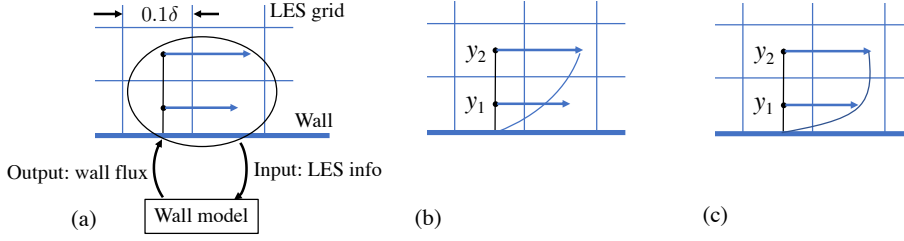


FIGURE 1. (a) Schematic of WMLES. (b) Schematic of the equilibrium wall model (EWM). The wall model (WM) and the LES match at the second off-wall grid point. (c) Schematic of the augmented WM. The WM and the LES match at two locations.

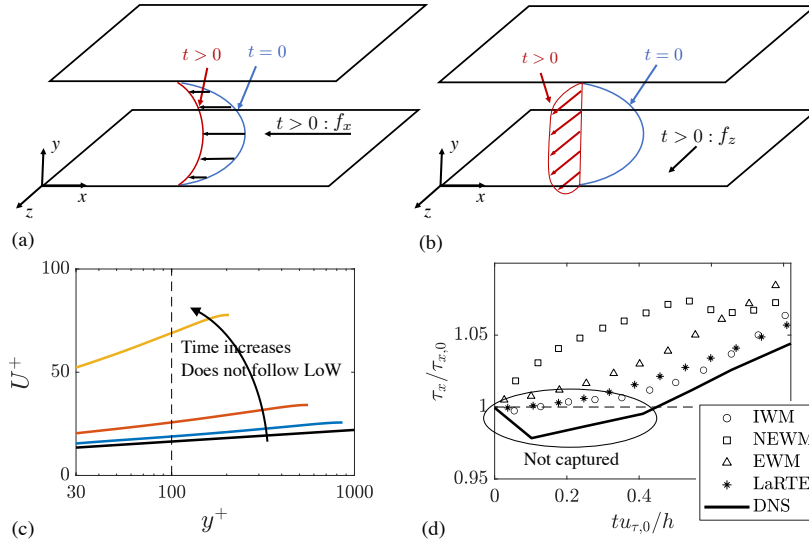


FIGURE 2. Schematics of a 2D channel subjected to (a) a suddenly imposed APG and (b) a suddenly imposed TPG at $t = 0$. Here, f_x and f_z are the imposed pressure gradients in the x and z -directions, t is the time, and x , y , and z are the Cartesian coordinates. (c) Evolution of the velocity profiles in time after an APG, $f_x = 100f_{x,0}$, is suddenly applied to a $Re_\tau = 1000$ channel. The black solid line corresponds to the log law $U^+ = \log(y^+)/\kappa + B$, where $\kappa = 0.4$ and $B = 5$. Here, Re_τ is the friction Reynolds number, $f_{x,0}$ is the driving force of the 2D channel, U is the streamwise velocity, and the superscript $+$ denotes normalization by wall units. (d) Evolution of the x -direction wall-shear stress after a TPG, $f_z = 10f_{z,0}$, is applied to a $Re_\tau = 10000$ channel. Data from Lozano-Durán *et al.* (2020) and Fowler *et al.* (2022). DNS: direct numerical simulation, IWM: integral wall model (Yang *et al.* 2015), NEWM: non-equilibrium wall model (Park & Moin 2014), EWM: equilibrium wall model (Yang *et al.* 2017), and LaRTE: Lagrangian relaxation towards equilibrium model (Fowler *et al.* 2022).

$Re_\tau = 1000$ channel. The wall-shear stress decreases and then increases. This behavior, however, is not captured by existing wall models.

This work aims to advance WMLESs by accounting for the aforementioned non-equilibrium effects. The basic idea is to augment the LoW such that the ansatz used for velocity reconstruction in the wall-adjacent cell(s) provides a more realistic description of the mean flow than the LoW. In other words, instead of employing the following ansatz

$$\mathbf{U} = \mathbf{c}_1 \text{LoW}(y^+), \quad (1.1)$$

as in the EWM, we employ

$$\mathbf{U} = \mathbf{c}_1 \text{LoW}(y^+) + \mathbf{c}_2 g(y^+), \quad (1.2)$$

where \mathbf{U} is the wall-modeled velocity; $g(y^+)$ is, at this point, a generic function; and \mathbf{c} 's are unknowns—notice that \mathbf{c}_1 and \mathbf{c}_2 have the dimension of velocity. One must know both \mathbf{c}_1 and \mathbf{c}_2 to determine y^+ and therefore both Eqs. (1.1) and (1.2) are implicit equations. The viscous-scaled distance from the wall y^+ is defined so long as the friction velocity is not 0. We will discuss the removable singularity of $\tau_w = 0$ in the next section.

Figure 1(b,c) is a schematic of the velocity reconstruction according to Eqs. (1.1) and (1.2). Yang *et al.* (2015) and Lv *et al.* (2021) argued that $g \sim y$ to leading order. Here, we get g from modal analysis, specifically, g is constructed from the first POD mode of the one-dimensional streamwise velocity profile along the wall-normal direction in a $Re_\tau = 5200$ channel. We make a distinction between this one-dimensional scalar form of POD and the conventional 3D vector variant. In the conventional approach, POD of the velocity vector in 3D is performed. The analysis yields 3D vector modes. The POD of the one-dimensional streamwise velocity profile is the POD of realizations $u(y)$. It yields one-dimensional scalar modes. Results of the former analysis can be found in, e.g., Hellström *et al.* (2016). There, the POD modes are not necessarily universal. The latter analysis was recently pursued systematically by Hansen *et al.* (2022), and the authors showed that the modes do not depend on the Reynolds number. Results in Hansen *et al.* (2022) are not included here for brevity.

2. Methodology

2.1. Wall-model formalism

Equation (1.2) has two modes, i.e., LoW and g . It must match at two off-wall locations to solve for $\mathbf{c}_1 = (c_{1x}, c_{1z})$ and $\mathbf{c}_2 = (c_{2x}, c_{2z})$,

$$\begin{aligned} c_{1x} \text{LoW}(y_1^+) + c_{2x} g(y_1^+) &= U_1, & c_{1z} \text{LoW}(y_1^+) + c_{2z} g(y_1^+) &= W_1, \\ c_{1x} \text{LoW}(y_2^+) + c_{2x} g(y_2^+) &= U_2, & c_{1z} \text{LoW}(y_2^+) + c_{2z} g(y_2^+) &= W_2. \end{aligned} \quad (2.1)$$

Here, y_1 and y_2 are wall-normal coordinates of the two matching locations, and $U_{1,2}$ and $W_{1,2}$ are the x - and z -direction LES velocities at the two matching locations. Following Yang *et al.* (2017), we filter the two velocities. The wall-shear stress is given by

$$\begin{aligned} \tau_x &= \nu \left. \frac{dU}{dy} \right|_{y=0} = \nu \left(c_{1x} \frac{d\text{LoW}}{dy^+} + c_{2x} \frac{dg}{dy^+} \right) \frac{dy^+}{dy} = \nu (c_{1x} + c_{2x}) \frac{u_\tau}{\nu} = (c_{1x} + c_{2x}) u_\tau, \\ \tau_z &= (c_{1z} + c_{2z}) u_\tau, \end{aligned} \quad (2.2)$$

where $d\text{LoW}/dy^+|_{y=0} = 1$ by definition, $dg/dy^+|_{y=0} = 1$ is enforced through properly normalizing g (detailed in Sec. 2.2), and $dy^+/dy = u_\tau/\nu$ by definition. The friction velocity u_τ in Eq. (2.2) is

$$u_\tau = (\tau_x^2 + \tau_z^2)^{1/4} = [(c_{1x} + c_{2x})^2 + (c_{1z} + c_{2z})^2]^{1/4} u_\tau^{1/2}, \quad (2.3)$$

i.e.,

$$u_\tau = [(c_{1x} + c_{2x})^2 + (c_{1z} + c_{2z})^2]^{1/2}. \quad (2.4)$$

Equations (2.1) and (2.4) are iteratively solved for the \mathbf{c} 's. Equation (2.2) is then invoked to compute the wall-shear stress. Note that the model reduces to the algebraic equilibrium wall model when $\mathbf{c}_2 = 0$.

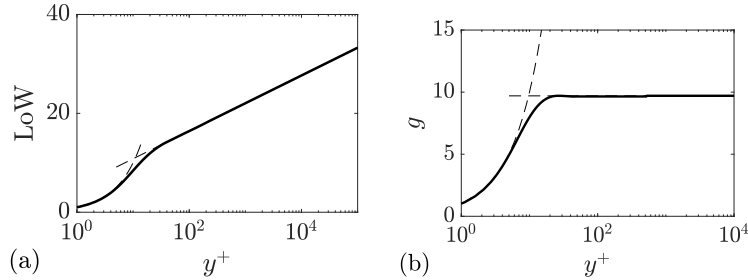


FIGURE 3. (a) The LoW mode. The two dashed lines correspond to $\text{LoW} = y^+$ and $\text{LoW} = \log(y^+)/\kappa + B$. (b) The g mode. The two dashed lines correspond to $g = y^+$ and $g = 9.7$.

2.2. Wall-model modes

Figure 3(a) shows the LoW mode, which is straightforward. The mode contains the viscous sublayer, the buffer layer, and the logarithmic layer, but not the wake layer. The behavior of the LoW mode conforms to $U^+ = \log(y^+)/\kappa + B$ at sufficiently large y^+ . The mode g takes more thinking. Define $\mathbf{r} = \mathbf{U} - \mathbf{c}_1 \text{LoW}$ to be the deviation from the LoW. The mode g is intended to capture \mathbf{r} , or at least part of \mathbf{r} . Any function, as long as it is not exactly the LoW, should capture part of \mathbf{r} . We want a mode that captures as much energy in \mathbf{r} as possible. This directly leads to POD. Here, we construct g based on the first POD mode of the one-dimensional streamwise velocity profile along the wall-normal direction in a $Re_\tau = 5200$ channel. Figure 3(b) shows the mode g . The mode is approximately a constant away from the wall and conforms to the no-slip condition at the wall. Notice that both the LoW and the mode g are linear functions of y^+ in the viscous layer. Hence, when the viscous length scale is large, Eqs. (1.2) and (2.1) degenerate to

$$(\mathbf{c}_1 + \mathbf{c}_2)y^+ = \mathbf{U}, \quad (2.5)$$

and $\mathbf{c}_1, \mathbf{c}_2$ are non-unique. This is not a limitation of the model though, because $\mathbf{c}_1 + \mathbf{c}_2$ is unique, and therefore the wall-shear stress is unique. The fact that the reconstruction in Eq. (1.2) degenerates to a linear reconstruction also takes care of the removable singularity of $\tau_w = 0$. ($\tau_w = 0$ is a singularity because y^+ is not defined when $\tau_w = 0$, and it is removable because it does not create mathematical singularities to the calculation of the wall-shear stress.) When implementing the wall model, we tabulate the LoW mode and the POD mode in a look-up table. An inquiry about LoW's and g 's values at a y^+ is interpolated from the look-up table.

We acknowledge that the POD modes in another flow will not be the same as the ones in a 2D channel, but we note that the POD modes in a 2D channel constitute a complete basis function set. Furthermore, we have the following considerations. First, the flow physics that governs the instantaneous flow in a channel is present in other wall-bounded flows; second, direct numerical simulation (DNS) data of channel flow are extensively available (Graham *et al.* 2016); and third, the g mode in Figure 3 is still a lot more physical than an arbitrarily picked polynomial.

3. Results

We apply the POD-augmented WM to 2D channels, and channels subjected to a suddenly imposed adverse or transverse pressure gradient.

Case	Re_τ	Grid	Domain	$\Delta z^+/2$	WM
R2N48	180	$96 \times 48 \times 96$	$2\pi \times 2 \times \pi$	1.88	POD-WM
R10N12	1000	$24 \times 12 \times 24$	$2\pi \times 2 \times \pi$	41.7	POD-WM
R1000N12	10^5	$24 \times 12 \times 24$	$2\pi \times 2 \times \pi$	4.17×10^3	POD-WM

TABLE 1. WMLES details. The half-channel height is used to normalize the numbers in the ‘‘Domain’’ column. The first off-wall grid point is at $\Delta_z/2$ (the half is because of the staggered grid).

3.1. Code

The POD-augmented WM is implemented in our in-house pseudo-spectral code LESGO. The code solves the incompressible Navier-Stokes equations in a half channel with a slip-top boundary and periodicity in both the streamwise and the spanwise directions. The flow is driven by a constant streamwise pressure gradient. The code employs a pseudo-spectral method in the streamwise and the transverse directions, a second-order finite difference method in the normal direction, and the second-order Adam-Bashforth method for time stepping. The grid is uniform in each direction. The time-step size is such that the CFL number is always smaller than 0.06. Last, the sub-grid scale (SGS) stresses are modeled via the Lagrangian scale-dependent model (Bou-Zeid *et al.* 2005). The code is well-validated (Abkar & Moin 2017; Yang *et al.* 2020, 2022), and further details of the code’s numerics can be found in Yang & Abkar (2018) and the references cited therein.

3.2. Fully developed channel

We apply the POD-augmented WM in 2D channels. This exercise will serve as validation: the WM must be able to predict the law of the wall at all Reynolds numbers on both wall-resolved and wall-modeled grids. Table 1 shows the details of the WMLESs. The nomenclature of the cases is R[$Re_\tau/100$]N[N_y]. The Reynolds number is from $Re_\tau = 180$ to 10^5 , the grid is from DNS-like (in case R2N48) to typical-WMLES-like (in cases R10N12 and R1000N12), and the domain is of the size of a minimum channel (Lozano-Durán & Jiménez 2014). The LES/WM matching location is at the first two off-wall grid points. The matching locations are in the viscous sublayer (in case R2N48) or the logarithmic layer (in cases R10N12 and R100N12). Following the established best practice (Larsson *et al.* 2016), the matching locations are not placed in the buffer layer. Figure 4(a) shows the mean flow. The profiles follow the LoW irrespective of the grid and the Reynolds number. Figure 4(b,c) shows the instantaneous contours of c_{1x} and c_{2x} . The mean flow is $U = u_\tau \text{LoW}(y^+)$ in a channel. Hence, c_{1x} ’s mean is u_τ , and c_{2x} ’s mean is 0. The above expectation bears out in Figure 4(b,c). Besides, any instantaneous deviation in c_{1x} from u_τ is a result of non-equilibrium effects, where we should see the mode g . This expectation also bears out in Figure 4(b,c).

3.3. Adverse pressure gradient

Next, we apply the POD-augmented WM in a channel subjected to a suddenly imposed APG. Figure 2(a) is a schematic of the flow. Figure 2(c) shows the time evolution of the mean flow. Table 2 shows the WMLES details. The nomenclature is R[$Re_\tau/100$]A [APG/ $(\tau_{w,0}/\delta)$], where the subscript 0 indicates a variable evaluated prior to the application of the APG. The channel is initially at a Reynolds number $Re_\tau = 1000$. The APGs are $10\tau_{w,0}/\delta$ and $100\tau_{w,0}/\delta$ in cases R10A10 and R10A100, respectively. The flow decelerates, and the Reynolds number decreases. LES information at the second and the fourth off-wall grid points are fed to the POD-WM so that we do not match in the buffer

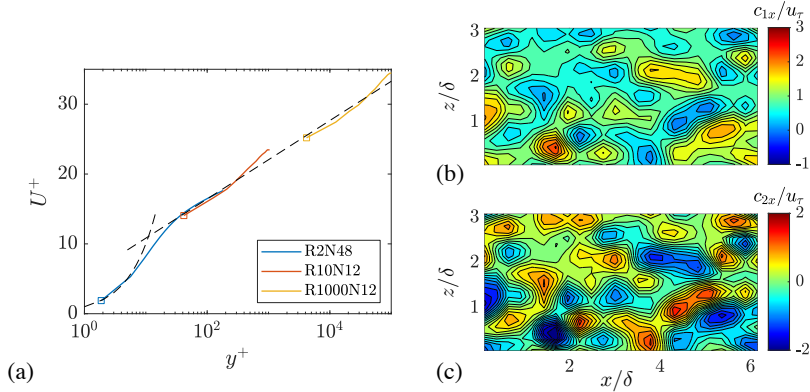


FIGURE 4. (a) Mean velocity profiles. The square symbols indicate the location of the first off-wall grid point. (b) Contours of c_{1x} . (c) Contours of c_{2x} .

Case	$Re_{\tau,0}$	Grid	Domain	APG	WM
R10A10	1000	$24 \times 12 \times 24$	$2\pi \times 2 \times \pi$	10	EWM, POD-WM
R10A100	1000	$24 \times 12 \times 24$	$2\pi \times 2 \times \pi$	100	EWM, POD-WM

TABLE 2. WMLES details. The half-channel height is used to normalize the numbers in the “Domain” column. The APG column shows the magnitude of the suddenly imposed APG. The numbers are normalized using $\tau_{w,0}/\delta$.

layer. For a fair comparison, the equilibrium WM (EWM) makes use of the LES information at these two off-wall locations as well: the EWM solves a wall-shear stress that yields the best fit of the velocity through the second and the fourth off-wall grid points.

Figures 5(a,b) shows the flow rate as a function of time for R10A10 and R10A100, respectively, and we compare WMLES and DNS. We generated the DNS data as well. The setups are similar to those in He & Seddighi (2015) and are not detailed here for brevity. We see from Figure 5(a,b) that the flow rate are accurately predicted irrespective of the wall model.

We explain why wall modeling is not critical to the prediction of the flow rate. The flow rate is governed by the volume integrated x momentum equation $d(\rho U_b)/dt = -\tau_w/\delta - dP/dx$. If the flow is inviscid, this equation becomes $d(\rho U_b)/dt = -dP/dx$, which leads directly to

$$U_b = U_{b,0} - \frac{1}{\rho} \frac{dP}{dx} t. \quad (3.1)$$

The above inviscid estimate is plotted in Figure 5(a,b) and is fairly accurate.

A more difficult test is the wall-shear stress. Figure 5(c,d) show the (horizontally averaged) wall-shear stress as a function of time for R10A10 and R10A100, respectively. The EWM captures the wall-shear stress in case R10A10 but grossly overpredicts the wall-shear stress in case R10A100. The POD-augmented WM, on the other hand, captures the wall-shear stress in both cases—although its prediction becomes less accurate as the flow approaches separation in case R10A100.

We explain why the POD-augmented WM is more accurate than the EWM. A wall model must rely on some mean flow scaling to predict the wall-shear stress. For example, the EWM relies on the LoW to predict wall-shear stress; the model gives accurate predictions of the skin friction in a channel because the LoW provides an accurate de-

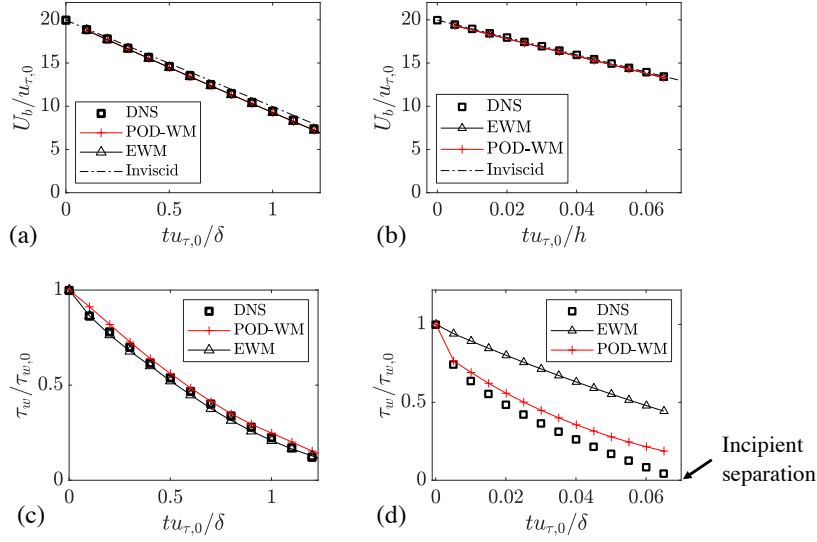


FIGURE 5. Flow rate as a function of time. (a) R10A10. (b) R10A100. Here, “Inviscid” corresponds to Eq. (3.1). Wall-shear stress as a function of time. (c) R10A10. (d) R10A100. DNS: values given by the DNS, which we take as the truth. POD-WM: predictions by the WMLES that employs the POD-augmented WM for near-wall turbulence modeling. EWM: predictions by the WMLES that employs the EWM for near-wall turbulence modeling.

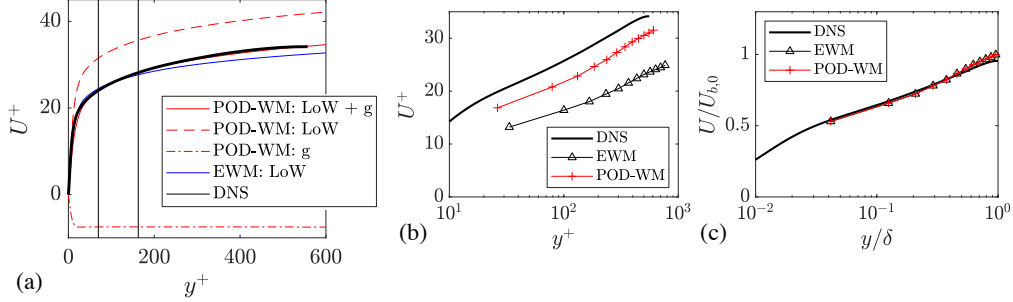


FIGURE 6. (a) DNS profiles and *a-priori* WM reconstructions at $tu_{\tau,0}/\delta = 0.035$ for case R10A100. The two vertical lines are at $1.5/12\delta$ and $3.5/12\delta$. The LoW mode and the g mode in the POD-augmented WM are also plotted. Their contributions to the wall-shear stress are of opposite signs, which is consistent with Figure 4. (b,c) Mean velocity profiles from DNS, WMLESs with EWM and POD-WM: (b) normalization by inner units and (c) normalization by outer units.

scription of the mean flow in a channel. Hence, a WM is accurate only if it is constructed based on an accurate mean flow scaling. Figure 6(a) shows the DNS velocity profile at $tu_{\tau,0}/\delta = 0.035$ in case R10A100 as well as the reconstructions of the mean velocity profiles according to the POD-augmented WM and the EWM. This is an *a-priori* test. The two WMs reconstruct the mean velocity profiles by matching the DNS profile at two y locations at $1.5/12\delta$ and $3.5/12\delta$. We see from Figure 6 that the POD-augmented WM provides a more accurate description of the mean flow than the EWM. This explains why the POD-augmented WM is more accurate.

Before we conclude this section, we comment on the presentation of the results. Figure

Case	$Re_{\tau,0}$	Grid	Domain	TPG	WM	N
R10T10	1000	$96 \times 12 \times 72$	$8\pi \times 2 \times 3\pi$	10	EWM, POD-WM	10

TABLE 3. WMLES details. The normalization is the same as in Table 2. N is the number of independent realizations.

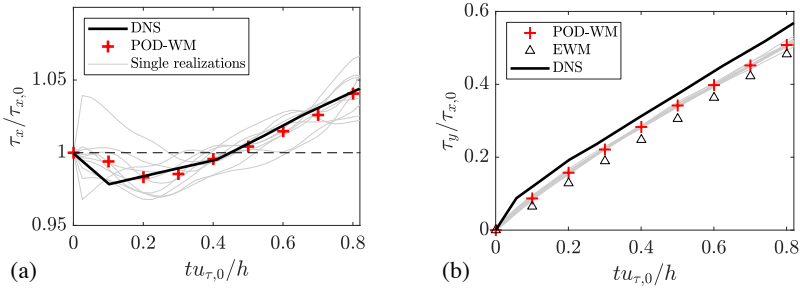


FIGURE 7. Time evolution of (a) the streamwise wall-shear stress and (b) the spanwise wall-shear stress. The DNS is by Lozano-Durán *et al.* (2020). The POD-WM results are ensemble averages from 10 statistically independent realizations.

6(b,c) show the DNS and WMLES profiles at $tu_{\tau,0}/\delta = 0.035$ in R10A100. At this time instant, the DNS predicts $\tau_w = 0.31\tau_{w,0}$. The POD-augmented WM predicts $\tau_w = 0.40\tau_{w,0}$, and the EWM predicts $\tau_w = 0.67\tau_{w,0}$, leading to a 116% error in EWM's prediction and a 29% error in POD-augmented WM's prediction. Hence, EWM is not at all accurate. This, however, is only clear from Figure 6(b), where normalization is by the inner units, not Figure 6(c), where normalization is by the outer units.

3.4. Transverse pressure gradient

Last, we apply the POD-augmented WM in a channel subjected to a suddenly imposed TPG. Figure 2(b) is a schematic of the flow. The channel is initially at a Reynolds number $Re_{\tau} = 1000$. The magnitude of the TPG = $10\tau_{w,0}/\delta$. Table 3 shows the WMLES details. Figures 7(a,b) shows the WMLES result. We observe the following. Firstly, the POD-augmented wall model captures the initial decrease in the x -direction wall-shear stress and gives wall-shear stress predictions that agree more closely with the DNS than the other models (comparing Figures 7 and 2(d)). Secondly, the x -direction wall-shear stress behaves differently from one realization to another, whereas the z -direction wall-shear stress behaves similarly from one realization to another. Thirdly, the POD-augmented WM gives more accurate z -direction wall-shear stress predictions than the EWM as well. Following the steps in Section 3.3, we can show that wall modeling is not critical to the prediction of the flow rate. We can also explain why the POD-augmented WM outperforms the EWM. These results, however, are not shown here for brevity.

4. Concluding remarks

We augment the LoW by including an additional mode that is based on the first POD mode in a 2D channel for LES wall modeling. The resulting wall model reconstructs the velocity in the wall layer according to

$$\mathbf{U} = \mathbf{c}_1 \text{LoW} + \mathbf{c}_2 g, \quad (4.1)$$

	moderate APG, 10	strong APG, 100	moderate TPG, 10
POD-WM	✓	✓	✓
EWM	✓	×	×

TABLE 4. A summary of the results. The number is the magnitude of the imposed pressure gradient, normalized by $\tau_{w,0}/\delta$. Here, ✓ and × indicate relatively good and relatively bad results, respectively.

where the LoW mode includes the viscous sublayer and the buffer layer, and g is the POD-based mode. The WM and LES match at two off-wall locations instead of one so that one can solve for \mathbf{c}_1 and \mathbf{c}_2 .

The results are promising. The POD-augmented WM captures the rapid decay of the wall-shear stress when a boundary-layer flow is subjected to a large APG. The model also captures the initial decrease in the streamwise wall-shear stress when a boundary-layer flow is subjected to a TPG. Both phenomena had not been captured in WMLES. *A priori* analysis shows that the POD-augmented WM captures these phenomena because its ansatz is a more realistic approximation of the mean flow when there is a pressure gradient. Table 4 summarizes the results. Although not shown here, favorable pressure gradients do not pose a challenge for wall modeling (Townsend 1956).

This work is a first attempt in applying results from modal analysis for predictive wall modeling in LES, and there is still a lot we can explore. Future work will explore WMs with more modes, modes from other modal analysis, and applications of the model in flows with complex geometries.

Acknowledgments

The authors thank Parviz Moin, Kevin Griffin, Ahmed Elnahhas, Rahul Agrawal, Adrian Lozano-Duran, H. Jane Bae, Michael Cui, Wen Wu, Olaf Marxen, and Mostafa Momen for their generous help during the CTR summer program.

REFERENCES

- ABKAR, M. & MOIN, P. 2017 Large-eddy simulation of thermally stratified atmospheric boundary-layer flow using a minimum dissipation model. *Boundary-Layer Meteorol.* **165**, 405–419.
- BOU-ZEID, E., MENEVEAU, C. & PARLANGE, M. 2005 A scale-dependent Lagrangian dynamic model for large eddy simulation of complex turbulent flows. *Phys. Fluids* **17**, 025105.
- DE VANNA, F., COGO, M., BERNARDINI, M., PICANO, F. & BENINI, E. 2021 Unified wall-resolved and wall-modeled method for large-eddy simulations of compressible wall-bounded flows. *Phys. Rev. Fluids* **6**, 034614.
- FOWLER, M., ZAKI, T. A. & MENEVEAU, C. 2022 A Lagrangian relaxation towards equilibrium wall model for large eddy simulation. *J. Fluid Mech.* **934**, A44.
- GOC, K. A., LEHMKUHL, O., PARK, G. I., BOSE, S. T. & MOIN, P. 2021 Large eddy simulation of aircraft at affordable cost: a milestone in computational fluid dynamics. *Flow* **1**, E14.
- GRAHAM, J., KANOV, K., YANG, X. I. A., LEE, M., MALAYA, N., LALESCU, C., BURNS, R., EYINK, G., SZALAY, A., MOSER, R. *et al.* 2016 A web services acces-

- sible database of turbulent channel flow and its use for testing a new integral wall model for LES. *J. Turbul.* **17**, 181–215.
- HANSEN, C., YANG, X. & ABKAR, M. 2022 Towards a non-equilibrium extension of the law of the wall in turbulent channel flows (in preparation).
- HE, S. & SEDDIGHI, M. 2015 Transition of transient channel flow after a change in Reynolds number. *J. Fluid Mech.* **764**, 395–427.
- HELLSTRÖM, L. H., MARUSIC, I. & SMITS, A. J. 2016 Self-similarity of the large-scale motions in turbulent pipe flow. *J. Fluid Mech.* **792**, R1.
- KAWAI, S. & LARSSON, J. 2012 Wall-modeling in large eddy simulation: Length scales, grid resolution, and accuracy. *Phys. Fluids* **24**, 015105.
- LARSSON, J., KAWAI, S., BODART, J. & BERMEJO-MORENO, I. 2016 Large eddy simulation with modeled wall-stress: recent progress and future directions. *Mech. Eng. Rev.* **3**, 15–00418.
- LOZANO-DURÁN, A., GIOMETTO, M. G., PARK, G. I. & MOIN, P. 2020 Non-equilibrium three-dimensional boundary layers at moderate Reynolds numbers. *J. Fluid Mech.* **883**, A20.
- LOZANO-DURÁN, A. & JIMÉNEZ, J. 2014 Effect of the computational domain on direct simulations of turbulent channels up to $Re_\tau = 4200$. *Phys. Fluids* **26**, 011702.
- LV, Y., HUANG, X. L. D., YANG, X. & YANG, X. I. A. 2021 Wall-model integrated computational framework for large-eddy simulations of wall-bounded flows. *Phys. Fluids* **33**, 125120.
- MONTY, J. P., HARUN, Z. & MARUSIC, I. 2011 A parametric study of adverse pressure gradient turbulent boundary layers. *Int. J. Heat Fluid Flow* **32**, 575–585.
- NA, Y. & MOIN, P. 1998 Direct numerical simulation of a separated turbulent boundary layer. *J. Fluid Mech.* **374**, 379–405.
- PARK, G. I. & MOIN, P. 2014 An improved dynamic non-equilibrium wall-model for large eddy simulation. *Phys. Fluids* **26**, 015108.
- TOWNSEND, A. 1956 The properties of equilibrium boundary layers. *J. Fluid Mech.* **1**, 561–573.
- VOLINO, R. J. 2020 Non-equilibrium development in turbulent boundary layers with changing pressure gradients. *J. Fluid Mech.* **897**, A2.
- YANG, X. I. A. & ABKAR, M. 2018 A hierarchical random additive model for passive scalars in wall-bounded flows at high Reynolds numbers. *J. Fluid Mech.* **842**, 354–380.
- YANG, X. I. A., CHEN, P. E., HU, R. & ABKAR, M. 2022 Logarithmic-linear law of the streamwise velocity variance in stably stratified boundary layers. *Boundary-Layer Meteorol.* **183**, 199–213.
- YANG, X. I. A. & GRIFFIN, K. P. 2021 Grid-point and time-step requirements for direct numerical simulation and large-eddy simulation. *Phys. Fluids* **33**, 015108.
- YANG, X. I. A., PARK, G. I. & MOIN, P. 2017 Log-layer mismatch and modeling of the fluctuating wall stress in wall-modeled large-eddy simulations. *Phys. Rev. Fluids* **2**, 104601.
- YANG, X. I. A., PIROZZOLI, S. & ABKAR, M. 2020 Scaling of velocity fluctuations in statistically unstable boundary-layer flows. *J. Fluid Mech.* **886**.
- YANG, X. I. A., SADIQUE, J., MITTAL, R. & MENEVEAU, C. 2015 Integral wall model for large eddy simulations of wall-bounded turbulent flows. *Phys. Fluids* **27**, 025112.